PHYSICAL REVIEW B VOLUME 39, NUMBER 5 15 FEBRUARY 1989-I

Pseudopotential approach to long-period narrow-gap superlattices

Jian-Bai Xia
Center of Theoretical Physics, Chinese Center of Advanced Science and Technology (World Laboratory), Beijing, China and Institute of Semiconductors, Chinese Academy of Sciences, P.O. Box 912, Beijing, China
(Received 25 July 1988)

The pseudopotential method is used to calculate the electronic structures of long-period narrow-gap InAs-GaSb and HgTe-CdTe superlattices. The variations of the energy gaps with the layer thicknesses and the band offsets, the subband dispersion along the k_x direction, the charge distributions along the lines connecting atoms in the [011] direction, and the optical-transition matrix elements are obtained. It is found that the crossing of the lowest electronic level and the highest hole level for the superlattice $(InAs)_n(GaSb)_n$ occurs at the period of 160 Å. The band offset has an essential effect on the energy gaps of the superlattice $(HgTe)_n(CdTe)_n$ with longer periods. The behavior of the interface states in the HgTe-CdTe superlattice is also discussed.

I. INTRODUCTION

In the last few years investigations of the electronic structures of narrow-gap semiconductor heterostructures (quantum wells, superlattices, etc.) have increased greatly,[1] because they are important for long-wavelength optoelectronic devices and far-infrared detectors, and because the quality of heterostructures involving narrow-gap materials has been significantly improved. The typical narrow-gap semiconductor superlattices InAs-GaSb and HgTe-CdTe involve type-II misaligned and type-III heterointerfaces, respectively.[2] Sai-Halasz *et al.*[3] first studied InAs-GaSb superlattices theoretically on the basis of Kane's two-band model,[4] and subsequently Sai-Halasz *et al.*,[5] Madhukar *et al.*,[6] and Chang *et al.*[7] performed tight-binding linear-combination-of-atomic-orbitals (LCAO) band calculations. These works indicated a strong dependence of the subband structure on the superlattice period. The semiconducting energy gap was found to decrease with increasing period, becoming zero at a certain value of the period (given as 120 Å in Ref. 3, as 230 Å in Ref. 5, and as 170 Å by Esaki[2]), leading thus to a semiconductor-to-semimetal transition. Bastard[8] later used an envelope-function approximation to calculate the electronic structures, and obtained that the crossing of the first electronic subband and the first heavy-hole subband occurs at a period of 230 Å. Altarelli[9] performed a self-consistent calculation of the electronic structure using the envelope-function approximation, and showed that when the wave vector is not equal to zero the wave functions will be hybridized to produce a small energy gap because of the mixing of the heavy and light holes. Therefore, the InAs-GaSb superlattices should always be semiconductors at low temperatures.

Schulman and McGill[10] pointed out that HgTe-CdTe superlattices were important as a new material for far-infrared detectors. Guldner *et al.*,[11] Chang *et al.*,[12] and Lin-Liu *et al.*[13] calculated the subband energies and dispersion in the HgTe-CdTe quantum wells, and noticed that there exist interface states satisfying the boundary conditions, because of the opposite signs of the light-hole effective masses in the two materials.

The above-mentioned calculations of the electronic structures are mainly based on the effective-mass theory and the tight-binding LCAO method. The effective-mass theory is more complicated in dealing with type-II and type-III superlattices than superlattices of type I. In general it has to consider the electron and hole states together, so that in order to calculate the in-plane subband dispersion it needs to solve an 8×8-dimensional combined differential equation. The difference between the effective-mass parameters in the two materials generally has to be taken into account, so that the kinetic-energy terms in the effective-mass equations should be symmetrized, and the boundary conditions of continuity of the wave-function derivatives be replaced by the conservation condition of particle flows.

In this paper we shall calculate the subband structures of long-period, narrow-gap superlattices by the pseudopotential method. The pseudopotential method has been applied to the calculation of electronic structures of superlattices for about ten years.[14–16] However, most calculations are limited to short-period superlattices because of the large unit cell of the superlattices. The author and Baldereschi[17] proposed a pseudopotential method to carry out calculations for long-period superlattices and used the method to calculate the electronic structure of $GaAs\text{-}Al_xGa_{1-x}As$ superlattice with a lattice period of 50 lattice constants. The pseudopotential calculations are carried out by a two-step procedure. In the first step, a usual pseudopotential calculation is made for an average lattice, with pseudopotentials which are weighted averages of the pseudopotentials of the component materials. In the second step, the Bloch solutions obtained in the first step are used as new basis in a calculation for the superlattice. The calculation method is presented in Sec. II. The results of InAs-GaSb and HgTe-CdTe superlattices are presented in Secs. III and IV, respectively.

II. CALCULATION METHOD

Let the pseudopotential of the A-B superlattice be

$$V(\mathbf{r})=\begin{cases}V_A(\mathbf{r}) & \text{in material } A\ ,\\ V_B(\mathbf{r}) & \text{in material } B\ ,\end{cases} \tag{1}$$

 ©1989 The American Physical Society

where $V_A(\mathbf{r})$ and $V_B(\mathbf{r})$ are the empirical pseudopotentials of A and B bulk materials, respectively,

$$\begin{aligned} V_A(\mathbf{r}) &= \sum_{\mathbf{q}} V_A(\mathbf{G}) e^{i\mathbf{G}\cdot\mathbf{r}} \\ &= \sum_{\mathbf{G}} [v_A^s(G)\cos(\mathbf{G}\cdot\tau) + i v_A^A(G)\sin(\mathbf{G}\cdot\tau)] e^{i\mathbf{G}\cdot\tau} , \\ V_B(\mathbf{r}) &= \sum_{\mathbf{G}} V_B(\mathbf{G}) e^{i\mathbf{G}\cdot\mathbf{r}} \\ &= \sum_{\mathbf{G}} [v_B^s(G)\cos(\mathbf{G}\cdot\tau) + i v_B^A(G)\sin(\mathbf{G}\cdot\tau)] e^{i\mathbf{G}\cdot\tau} . \end{aligned} \tag{2}$$

v_A^s, v_A^A, v_B^s, and v_B^A are the symmetrical and antisymmetrical form factors of the atomic pseudopotentials[18] in two materials. The origin is placed at the midpoint between the cation and anion. The $\mathbf{G}$'s are the reciprocal-lattice vectors of the single crystal; in the following we shall use $\mathbf{g}$'s to express the reciprocal-lattice vectors of the superlattice.

We expand the wave function of the superlattice with plane waves,

$$\psi_{\mathbf{k}}(\mathbf{r}) = \frac{1}{\sqrt{V}} \sum_{\mathbf{g}} c_{\mathbf{g}} e^{i(\mathbf{k}+\mathbf{g})\cdot\mathbf{r}} , \tag{3}$$

where $\mathbf{k}$ is a wave vector in the Brillouin zone of the superlattice. For the superlattice $(A)_m(B)_n$, and the origin placed at the center of the A material, the matrix elements of the superlattice pseudopotential can be written as

$$\langle \mathbf{k}+\mathbf{g} | V(\mathbf{r}) | \mathbf{k}+\mathbf{g}' \rangle = \begin{cases} \alpha V_A(\Delta\mathbf{g}) + (1-\alpha) V_B(\Delta\mathbf{g}), & \Delta\mathbf{g} = \mathbf{G} \\ \sum_{G_z} [V_A(\Delta g_x, \Delta g_y, G_z) - V_B(\Delta g_x, \Delta g_y, G_z)] \frac{2}{L} \frac{\sin(G_z - \Delta g_z)\frac{W}{2}}{G_z - \Delta g_z} e^{i(G_z - \Delta g_z)(a/8)}, & \Delta\mathbf{g} \neq \mathbf{G} \end{cases} \tag{4}$$

where $\Delta\mathbf{g} = \mathbf{g} - \mathbf{g}'$, $\alpha = m/(m+n)$, and $V_A(\mathbf{G})$ and $V_B(\mathbf{G})$ are given by Eq. (2). If we take an average virtual-crystal potential

$$V_0(\mathbf{r}) = \alpha V_A(\mathbf{r}) + (1-\alpha) V_B(\mathbf{r}) \tag{5}$$

as the zero approximation of the superlattice pseudopotential, the corresponding Bloch functions with wave vectors

$$\mathbf{k}_i = \mathbf{k} + \frac{2\pi i}{L}\hat{\mathbf{z}}, \quad i = 0, \pm 1, \pm 2, \ldots \tag{6}$$

are taken as basic functions $\psi_{l,\mathbf{k}_i}(\mathbf{r})$. Then the wave functions can be expressed as

$$\psi_{\mathbf{k}}(\mathbf{r}) = \sum_{l,\mathbf{k}} C_{li} \psi_{l,\mathbf{k}_i}(\mathbf{r}) . \tag{7}$$

By using (7) instead of (3) the dimension of the secular equation can be reduced greatly. In general, for each $\mathbf{k}_i$ it is enough to take ten alloy states (including four valence states and six conduction states) to obtain convergent results.[17] In principle the number of $\mathbf{k}_i$ in Eq. (6) should be $m+n$, but for long-period superlattices it has been proved in Ref. 17 that eleven $\mathbf{k}_i$'s are enough to obtain convergent ground and low-energy excited states in the quantum well. Therefore the dimension of the resulting secular equation becomes (number of $\mathbf{k}_i$)$\times$(number of alloy states at each $\mathbf{k}_i$).

The spin-orbital interaction is considered following Weisz[19] and Chelikowsky's[20] method, and the spin-orbital Hamiltonian is written as

$$H_{\mathbf{k}\mathbf{k}'}^{\text{s.o.}} = (\mathbf{k}\times\mathbf{k}')\cdot\sigma_{ss'} \left[-\frac{i}{2(m+n)} \sum_j \lambda_j e^{-i(\mathbf{k}-\mathbf{k}')\cdot\tau_j} \right] , \tag{8}$$

where $\sigma_{ss'}$ is Pauli's spin matrix,

$$\lambda_j = \mu_j B_{nl}^j(k) B_{nl}^j(k') , \tag{9}$$

and the μ_j are adjustable parameters, so that the ratio of μ_c and μ_a for cations and anions equals that of the spin-orbit splitting for free atoms.[21] The B_{nl} are defined as

$$B_{nl}(k) = \beta \int_0^\infty j_{nl}(kr) R_{nl}(r) r^2 dr , \tag{10}$$

R_{nl} is the radial wave function of the outermost p orbital in the closed shell of the atomic core, and β is a normalization constant satisfying

$$\lim_{k\to 0} k^{-1} B_{nl}(k) = 1 . \tag{11}$$

Finally the virtual-crystal Hamiltonian including the spin-orbit interaction is expressed as

$$\begin{aligned} H_0 = \frac{p^2}{2m} &+ \alpha V_A(\mathbf{r}) + (1-\alpha) V_B(\mathbf{r}) \\ &+ (\mathbf{k}\times\mathbf{k}')\cdot\sigma_{ss'}(-i)[\alpha\lambda_A(\mathbf{k}-\mathbf{k}') \\ &+ (1-\alpha)\lambda_B(\mathbf{k}-\mathbf{k}')] , \end{aligned} \tag{12}$$

where

$$\lambda_A(\mathbf{g}) = \lambda_A^s(g)\cos(\mathbf{g}\cdot\tau) + i\lambda_A^A(g)\sin(\mathbf{g}\cdot\tau) . \tag{13}$$

$\lambda_B(\mathbf{g})$ is defined similarly.

III. RESULTS FOR THE InAs-GaSb SUPERLATTICE

We use the pseudopotential form factors of InAs and GaSb given by Ref. 18, and adjust the $V^s(0)$ so that the energy of the valence-band top of GaSb is higher than that of the conduction-band bottom of InAs by 0.15 eV,

TABLE I. Energy-band parameters of InAs and GaSb.

	Lattice constant (Å)						
	6.08						
	Pseudopotential form factors (Ry)						
	$V^s(0)$	$V^s(3)$	$V^s(8)$	$V^s(11)$	$V^A(3)$	$V^A(4)$	$V^A(11)$
InAs	0.00	−0.22	0.0012	0.05	0.08	0.05	0.03
GaSb	0.02	−0.22	0.008	0.05	0.06	0.05	0.01
	Spin-orbit parameters						
	In	As	Ga	Sb			
μ_j	0.002 37	0.002 20	0.001 27	0.007 21			
	Energies at Γ point (eV)						
	Γ_7	Γ_8	Γ_6				
InAs	6.6766	7.0566	7.4739				
GaSb	6.8732	7.6232	8.4339				

which is in agreement with experimental results.[22,23] The pseudopotential form factors, spin-orbit parameters, and the calculated energies at the Γ point of InAs and GaSb are given in Table I.

The k_x subbands of $(InAs)_{30}(GaSb)_{30}$ are shown in Fig. 1. From the figure we see that all the energy levels are spin split, which is caused by the lack of inversion symmetry in group-III-V compounds. In the effective-mass theory it is expressed by a linear term of $\mathbf{k}$ in the effective-mass Hamiltonian, which is often omitted. At $\mathbf{k}=0$ this energy splitting for the heavy-hole states and $n \geq 3$ electronic states is generally smaller than 1 meV, and that of the $n=1,2$ electronic and the first light-hole states are 7, 2, and 9 meV, respectively. From these values the linear term in the effective-mass Hamiltonian can be evaluated.

The assigned characters of the energy levels at $\mathbf{k}=0$, as indicated in Fig. 1, are determined from the components of the predominant $\psi_{l,\mathbf{k}_i}$ included in the wave function and the number of nodes of the wave function along the z direction. From Fig. 1 we see that at $\mathbf{k}=0$ the first electronic energy level $E1$ is located below the heavy-hole levels $H1$ and $H2$. This is in agreement with theoretical results reported in the literature.

In the $k_x \neq 0$ direction, because of the interaction between the heavy-hole and electronic subbands, the energy levels $H1$, $H2$, and $E1$ hybridize strongly at

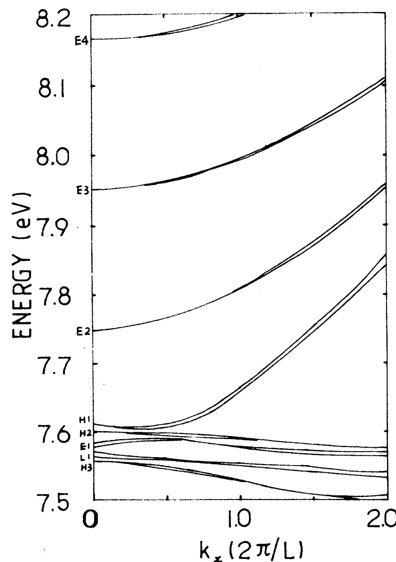

FIG. 1. Subband dispersion of the superlattice $(InAs)_{30}(GaSb)_{30}$ along the k_x direction.

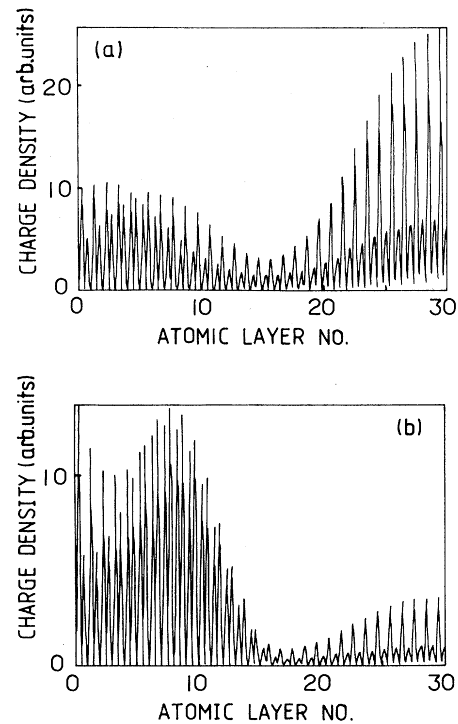

FIG. 2. Charge distributions of the superlattice $(InAs)_{30}(GaSb)_{30}$ at $k_x=\pi/L$. (a) Lowest electronic state. (b) Highest hole state. The left-hand side is GaSb, the right-hand side is InAs.

$k_x = 0.5(2\pi/L)$, resulting in a small energy gap of 4.51 meV. The energy separation between the conduction-band bottom at $k_x = 0.5(2\pi/L)$ and the valence-band top at $\mathbf{k}=\mathbf{0}$ is about 1 meV; this is the indirect energy gap of the superlattice.

We have also calculated the electronic distributions along the lines connecting cations and anions in the [011] direction from the wave functions. The localization of the electronic and the hole distributions in the InAs and GaSb layers, respectively, are seen obviously. But at $k_x = 0.5(2\pi/L)$, because of the strong hybridization between energy levels, some states have their distributions extended over the whole superlattice. Figure 2 shows the charge distributions of the lowest conduction state and highest valence state at $k_x = \pi/L$ along the line connecting atoms. It is a half-period of the superlattice $(InAs)_{30}(GaSb)_{30}$, where the left part is GaSb and the right part is InAs.

When the number of atomic layers of the superlattices $(InAs)_n(GaSb)_n$ decreases, the electronic energy level $E1$ will rise gradually and become higher than the heavy-hole level $H1$. For the n (or period L) at which this crossing occurs, different calculations give different results (see Introduction). We have calculated the subband energies of $(InAs)_n(GaSb)_n$ superlattices at $\mathbf{k}=\mathbf{0}$ for different values of n, with the results shown in Fig. 3. From the figure we see that the crossing occurs at $n=26$, i.e., $L = 160$ Å.

We have also calculated the optical-transition matrix elements of the superlattices from the wave functions,

$$Q_{nn',i}(\mathbf{k}) = \frac{2}{m} |\langle n,\mathbf{k}|p_i|n',\mathbf{k}\rangle|^2, \quad i=x,y,z \tag{14}$$

where p_i are the components of the momentum operator in the x, y, and z directions, and n and n' represent the electronic and hole states, respectively. In calculating Eq. (14) we sum over all the contributions from the two spin-degenerate states of each state and average the transition matrix elements in the x and y directions. Tables II and III give the optical-transition matrix elements in $(InAs)_{14}(GaSb)_{14}$ at $\mathbf{k}=(0,0,0)$, and $\mathbf{k}=(0,0,\pi/L)$, respectively. From the tables we see that the transition probabilities are generally smaller than that of type-I superlattices (for the $GaAs\text{-}Al_{0.2}Ga_{0.8}As$ superlattice, $Q_{nn'} \sim 20$ eV),[17] but there are still very appreciable transition probabilities in many cases. Comparing Tables II and III we find that the Δn selection rules of even and odd parity are reversed for $\mathbf{k}=\mathbf{0}$ [the center of the Brillouin zone (BZ)] and $k_z = \pi/L$ (the edge of the BZ). This is caused by localization of the electron and hole in different materials, as was first noted by Voisin *et al.*[24] Experimentally Voisin *et al.*[25] have observed the low-temperature photoluminescence spectra of a (30–50)-Å InAs-GaSb superlattice, which has a peak at about 265 meV. From our calculation of $(InAs)_{10}(GaSb)_{16}$, the transition energies from electronic $E1$ state to heavy hole $H1$ and to light hole $L1$ states are 233 and 309 meV, respectively.

TABLE II. Optical-transition matrix elements of $(InAs)_{14}(GaSb)_{14}$ at $\mathbf{k}=(0,0,0)$. The first line is Q_{xy}, the second is Q_z (in units of eV).

	$E1$	$E2$	$E3$
$H1$	1.1433	0.0084	6.4922
	0.0222	0.0006	0.0114
$H2$	0.0454	1.9080	0.1650
	0.6125	0.0008	0.3889
$L1$	0.6859	0.1540	2.5259
	7.3014	0.0010	4.7773
$H3$	1.0518	0.0138	1.3256
	0.0006	0.0035	0.0003

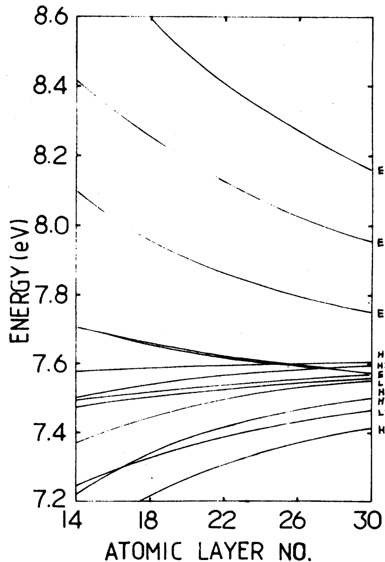

FIG. 3. Variation of the energy levels of the superlattice $(InAs)_n(GaSb)_n$ at $\mathbf{k}=\mathbf{0}$ with n.

IV. RESULTS FOR THE HgTe-CdTe SUPERLATTICE

We use the pseudopotential form factors of HgTe and CdTe given in Ref. 26. The pseudopotential form factors, spin-orbit parameters, and the energies of HgTe and CdTe at the Γ point used in our calculation are shown in Table IV. Because the band offset of the HgTe-CdTe superlattice has not been uniquely determined by experiments or theories,[27] we shall carry out calculations for assumed values of band offset [by corresponding choice of

TABLE III. Optical-transition matrix elements of $(InAs)_{14}(GaSb)_{14}$ at $\mathbf{k}=(0,0,\pi/L)$ (in units of eV).

	$E1$	$E2$	$E3$
$H1$	0.0011	2.5615	0.0094
	0.0004	0.0002	0.0001
$H2$	0.6785	0.0060	3.5629
	0.0005	0.0035	0.0001
$L1$	0.0027	1.1978	0.0142
	0.0092	1.8905	0.0033
$H3$	0.0090	1.7630	0.0454
	0.0388	0.0002	0.0103

TABLE IV. Energy-band parameters of HgTe and CdTe.

Lattice constant (Å)							
				6.471			
	Pseudopotential form factors (Ry)						
	$V^s(3)$	$V^s(8)$	$V^s(11)$	$V^A(3)$	$V^A(4)$	$V^A(11)$	$V^A(12)$
HgTe	−0.262	−0.035	0.05	0.10	0.042	0.02	0.019
CdTe	−0.200	−0.012	0.027	0.168	0.075	0.028	0.0
	Spin-orbit parameters						
	Hg	Te	Cd	Te			
μ_j	0.004 35	0.006 37	0.000 89	0.004 96			
	Energies at Γ point (eV)						
	Γ_7	Γ_8	Γ_6				
HgTe	3.3890	4.3290	4.0238				
CdTe	3.4004	4.3104	5.6637				

$V^s(0)$ in HgTe].

First, we calculate the energy levels and wave functions of $(\mathrm{HgTe})_m(\mathrm{CdTe})_n$ at $\mathbf{k}=0$, for two different valence-band–offset values, namely 40 and 340 meV. The subband energies at $\mathbf{k}=0$ and band gaps are given in Table V. From the table we see that when the band offset increases from 40 to 340 meV, the energy gap decreases for the superlattices of longer periods. Wu *et al.*[28] calculated the variation of the energy gap with the band offset for the superlattice $(\mathrm{HgTe})_{50\,\text{Å}}(\mathrm{CdTe})_{50\,\text{Å}}$, and obtained that the energy gap decreases with an increase of ΔE_v. When the number of atomic layers n decreases from 30 to 14, the energy gap of the superlattice $(\mathrm{HgTe})_n(\mathrm{CdTe})_n$ increases. For $\Delta E_v=40$ meV the energy gap increases from 63 to 176 meV; for $\Delta E_v=340$ meV it increases from 28 to 156 meV. If we fix the number of HgTe atomic layers and reduce the number of CdTe atomic layers, the energy gap decreases. Reno *et al.*[29] have carried out magneto-optical measurements on HgTe-CdTe superlattices and obtained the relationship between the energy gap and the layer thickness. According to their calculation the superlattice will be semimetallic at low temperatures if the band offset is taken to be $\Delta E_v=350$ meV. But, from our calculation, if $\Delta E_v=340$ meV the superlattice $(\mathrm{HgTe})_{30}(\mathrm{CdTe})_{10}$ still has an energy gap of 34 meV (see Table V). Because our calculation is for the superlattice grown in the [001] direction and the real superlattices HgTe-CdTe generally are grown in the [111] direction, our results cannot be compared with experiments directly. However, the variation of the energy gaps with the layer thicknesses are basically in agreement with the experimental results, and the effect of the band offset may be important in comparing the theoretical and experimental results.

In order to identify interface states and noninterface states, we calculate the charge distributions along the lines connecting atoms in the [011] direction. Figure 4 gives in envelope form the charge distributions of the $\mathbf{k}=0$ states of various electron and hole subbands, for $(\mathrm{HgTe})_{30}(\mathrm{CdTe})_{30}$ and $(\mathrm{HgTe})_{30}(\mathrm{CdTe})_{10}$ assuming $\Delta E_v=40$ meV. From the figure we see that for $(\mathrm{HgTe})_{30}(\mathrm{CdTe})_{30}$, $E1$ and $H1$ are interface states, $E2$, $H2$, and $H3$ are bulk states localized in HgTe, and $H4$ is a state intermediate between the two kinds of states. For $(\mathrm{HgTe})_{30}(\mathrm{CdTe})_{10}$ the interface states are basically distributed in the CdTe layer, because the CdTe layer is thin. $E1$, $H1$, $H2$, and $H3$ belong to this kind of state, $H4$ is a bulk state localized in HgTe, and $E2$ extends over the

TABLE V. Energies and energy gaps of superlattices $(\mathrm{HgTe})_m(\mathrm{CdTe})_n$ at $\mathbf{k}=0$. Each energy represents the average energy of two spin states (in units of eV).

m of HgTe:	30	30	30	30	22	22	14	14
n of CdTe:	30	30	10	10	22	22	14	14
Assumed offset:	0.040	0.340	0.040	0.340	0.040	0.340	0.040	0.340
$E4$	5.121	5.381	4.972	5.249	5.348	5.603	5.806	6.021
$E3$	4.923	5.201	4.790	5.065	5.091	5.361	5.434	5.679
$E2$	4.471	5.011	4.636	4.891	4.844	5.109	5.062	5.316
$E1$	4.576	4.834	4.540	4.739	4.616	4.868	4.706	4.949
$H1$	4.513	4.806	4.494	4.705	4.517	4.801	4.530	4.793
$H2$	4.505	4.804	4.479	4.700	4.501	4.794	4.497	4.775
$H3$	4.497	4.784	4.432	4.691	4.484	4.762	4.456	4.717
$H4$	4.488	4.759	4.400	4.680	4.475	4.747	4.451	4.704
Gap	0.063	0.028	0.046	0.034	0.099	0.067	0.176	0.156

TABLE VI. Optical-transition matrix elements of $(HgTe)_{30}(CdTe)_{30}$ at $\mathbf{k}=0$ (in units of eV).

	$E1$	$E2$	$E3$	$E4$
$H1$	0.2453	2.8379	0.0801	0.3722
	0.6741	0.0002	0.0824	0.0001
$H2$	1.7729	0.0762	0.7489	0.0083
	0.0109	0.0092	0.0026	0.0041
$H3$	0.3442	0.7446	0.1031	1.8104
	0.8508	0.0023	0.1646	0.0011
$H4$	0.6757	0.0120	3.2847	0.0041
	0.0068	0.1251	0.0013	0.0060

whole superlattice.

Because of the complex nature of the states, the optical-transition matrix elements do not show obvious selection rules. Table VI gives the optical-transition matrix elements at $\mathbf{k}=0$ in $(HgTe)_{30}(CdTe)_{30}$, assuming $\Delta E_v = 40$ meV. Figure 5 shows the subband dispersion in the k_x direction of the superlattice $(HgTe)_{30}(CdTe)_{30}$. From the figure we see that the hole subbands are relatively even, and some subbands have large spin splittings at $k_x \neq 0$ because of the interaction between the interface and bulk states.

V. SUMMARY

In this paper we use the pseudopotential method developed for calculations with long-period superlattices[17] to calculate the electronic structure of long-period narrow-gap InAs-GaSb and HgTe-CdTe superlattices.

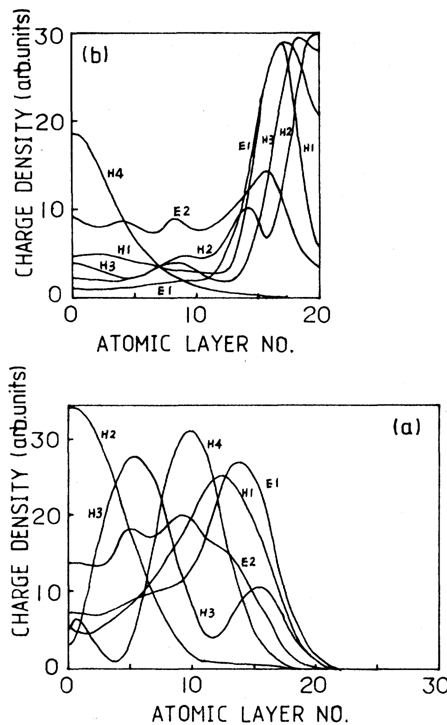

FIG. 4. Envelope forms of the charge distributions of the states at $\mathbf{k}=0$. (a) For $(HgTe)_{30}(CdTe)_{30}$. (b) For $(HgTe)_{30}(CdTe)_{10}$. The left-hand side is HgTe, the right-hand side is CdTe.

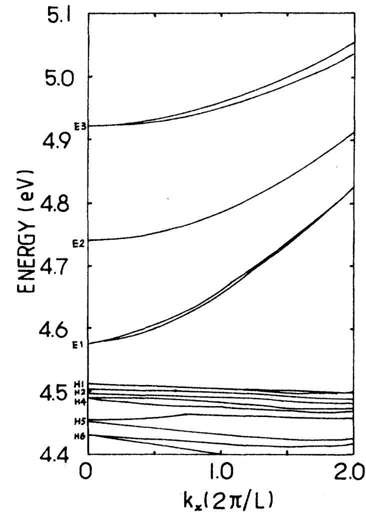

FIG. 5. Subband dispersion of the superlattice $(HgTe)_{30}(CdTe)_{30}$ along the k_x direction.

First, we assume that the pseudopotentials in the two materials of the superlattice are the empirical pseudopotentials in the two bulk materials, respectively, neglecting the variation of the pseudopotential near the interface. The band offset is given by experiments or assumption. Then we divide the pseudopotential of the superlattice into two parts: the alloy's and perturbation pseudopotentials. If the superlattice is $(A)_m(B)_n$, the alloy's pseudopotential is that of $A_{m/(m+n)}B_{n/(m+n)}$ in the virtual-crystal approximation. The wave functions of the superlattice are expanded with the eigen-wave-functions of the alloy at the $\mathbf{k}_i$ points [Eq. (6)]. By means of this the pseudopotential method can be extended to the calculation of long-period superlattices, and the labor of the calculation does not increase much.

For an InAs-GaSb superlattice we obtained the variation of the electronic and hole energy levels at $\mathbf{k}=0$ with the number of atomic layers $m=n$, and found that when $m=n=26$, i.e., the superlattice period equals to 160 Å, the first electronic and the first hole energy levels cross. When the superlattice period is greater than 160 Å, the first electronic energy level is located below the first hole energy level, and the superlattice becomes semimetallic. However, from the subband dispersion at $k_x \neq 0$ it is found that there is a small energy gap of ~ 1 meV due to the interaction between the electronic and hole subbands as they cross. The spin splittings of the levels are obvious because of the lack of inversion symmetry in group-III-V compounds. Except in the case of strong interaction, the electron and hole are well confined in the InAs and GaSb layers, respectively, and the InAs-GaSb superlattice has the character of the type-II superlattice. The optical-transition matrix elements of this superlattice are smaller than that of the type-I superlattice, but still have appreciable values. At $\mathbf{k}=0$ the selection rule of the optical-transition is Δn is even, and at $k_z=\pi/L$, Δn is odd.

For a HgTe-CdTe superlattice, because of the uncertainty of the band offset we took two values of the band offset, 40 and 340 meV, in the calculation in order to

study the effect of the band on the subband structures. It is found that the band offset has a more obvious effect on the energy gap of the long-period superlattice. Therefore, the experimental measurement of the energy gaps will be helpful to determine the band offset. From the density distribution of the electron and hole the interface states can be observed; meanwhile, the bulk-confined states and the states of both interface- and bulk-confined properties also exist. Thus it is difficult to designate the hole energy levels as heavy or light hole, just like the other type-I or -II superlattices. If the CdTe layer is thin, the interface states become bulk states localized in the CdTe layers. From the subband dispersion at $k_x \neq 0$ it is seen that the hole subbands are relatively even and have large spin splitting in some parts due to the interaction between the interface- and bulk-confined states. Because of the complexity of coexistence of the two kinds of states, the optical-transition matrix elements do not show obvious selection rules.

[1]G. Bastard, J. A. Brum, and J. M. Berroir, in *Optical Properties of Narrow-Gap Low-Dimensional Structures,* edited by C. M. Sotomayor Torres *et al.* (Plenum, New York, 1986), p. 1.
[2]L. Esaki, IEEE J. Quantum Electron. **QE-22**, 1611 (1986).
[3]G. A. Sai-Halasz, R. Tsu, and L. Esaki, Appl. Phys. Lett. **30**, 651 (1977).
[4]E. O. Kane, J. Phys. Chem. Solids **1**, 249 (1957).
[5]G. A. Sai-Halasz, L. Esaki, and W. A. Harrison, Phys. Rev. B **18**, 2812 (1978).
[6]A. Madhukar and R. N. Nucho, Solid State Commun. **32**, 331 (1979).
[7]Y. C. Chang and J. N. Schulman, Phys. Rev. B **31**, 2069 (1985).
[8]G. Bastard, Phys. Rev. B **24**, 5693 (1981).
[9]M. Altarelli, Phys. Rev. B **28**, 842 (1983).
[10]J. N. Schulman and T. C. McGill, Appl. Phys. Lett. **34**, 663 (1979).
[11]Y. Guldner, G. Bastard, J. P. Vieren, M. Voos, J. P. Faurie, and A. Million, Phys. Rev. Lett. **51**, 907 (1983).
[12]Y. C. Chang, J. N. Schulman, G. Bastard, Y. Guildner, and M. Voos, Phys. Rev. B **31**, 2557 (1985).
[13]Y. R. Lin-Liu and L. J. Sham, Phys. Rev. B **32**, 5561 (1985).
[14]W. E. Pickett, S. G. Louie, and M. L. Cohen, Phys. Rev. B **17**, 815 (1978).
[15]Ed Caruthers and P. J. Lin-Chung, Phys. Rev. B **17**, 2705 (1978).
[16]J. Ihm, P. K. Lam, and M. L. Cohen, Phys. Rev. B **20**, 4120 (1979).
[17]J. B. Xia and A. Baldereschi, Chin. J. Semicond. **8**, 574 (1987); see also Chin. Phys. (to be published).
[18]M. L. Cohen and V. Heine, in *Solid State Physics,* edited by F. Seitz and D. Turnbull (Academic, New York, 1970), Vol. 24, p. 37.
[19]G. Weisz, Phys. Rev. **149**, 504 (1966).
[20]J. R. Chelikowsky and M. L. Cohen, Phys. Rev. B **14**, 556 (1976).
[21]F. Herman, C. D. Kuglin, K. F. Cuff, and R. L. Kortum, Phys. Rev. Lett. **11**, 541 (1963).
[22]G. A. Sai-Halasz, L. L. Chang, J. M. Welter, C. A. Chang, and L. Esaki, Solid State Commun. **27**, 935 (1978).
[23]G. J. Gualtieri, G. P. Schwartz, R. G. Nuzzo, R. J. Malik, and J. F. Walker, J. Appl. Phys. **61**, 5337 (1987).
[24]P. Voisin, G. Bastard, and M. Voos, Phys. Rev. B **29**, 935 (1984).
[25]P. Voisin, in *Optical Properties of Narrow-Gap Low-Dimensional Structures,* Ref. 1, p. 85.
[26]D. J. Chadi, J. P. Walter, and M. L. Cohen, Phys. Rev. B **5**, 3058 (1972).
[27]J. P. Faurie, in *Optical Properties of Narrow-Gap Low-Dimensional Structures,* Ref. 1, p. 25.
[28]G. Y. Wu and T. C. McGill, J. Appl. Phys. **58**, 3914 (1985).
[29]J. Reno, I. K. Sou, J. P. Faurie, J. M. Berrior, Y. Guldner, and J. P. Vieren, Appl. Phys. Lett. **49**, 106 (1986).